Quadratic Synthesis of Integrated Active Controls for an Aeroelastic Forward-Swept-Wing Aircraft

M. G. Gilbert,* D. K. Schmidt,† and T. A. Weisshaar‡
Purdue University, West Lafayette, Indiana

The flexible wing structure and unconventional geometry of high performance, forward-swept-wing (FSW) aircraft are known to cause significant coupling between the flight mechanic and structural dynamic modes. Because of this coupling, an integrated approach to active stability augmentation synthesis and aeroelastic stabilization may be desirable. In this paper, quadratic synthesis is used to obtain pitch-rate-command flight control laws for evaluation. Ignoring the elastic modes in synthesizing these control laws is shown to lead to very unsatisfactory results. Inclusion of these modes directly in the synthesis is shown to yield significantly improved performance, thus suggesting an integrated approach at the outset rather than attempt to "tune" the design later in an aeroservoelastic analysis. Finally, modal analysis is used to show that the elastic modes are highly controllable with the canard surface on this configuration, thus leading to a need for a multivariable control approach.

Introduction

SINCE the concept of an aircraft with forward-swept wings was revived by Krone[1,2] a large amount of effort has been devoted to the study of the passive control of wing divergence through composite material structural tailoring. The superior performance and other potential benefits of this aircraft, including configuration flexibility; higher maneuver L/D; lower trim drag; very low stall speeds; improved handling at low speeds; and resistance to spin entry continues to interest vehicle designers.

Recent studies by Miller et al.[3] and Weisshaar et al.[4,5] have shown that the critical mode of instability for a forward-swept-wing aircraft is not likely to be wing divergence. Instead the loss of aeroelastic stiffness of the swept-forward wing that occurs at high speeds leads to increased cross coupling between flight mechanics modes and flexible modes of the structure. Accounted for improperly, this coupling can cause serious problems. Treated correctly, however, the coupling actually may be used to advantage.

The results of an investigation of aeroelastic coupling and active stabilization systems are presented here. Using a generic, statically unstable, forward-swept-wing fighter class aircraft with canard control surfaces, a series of longitudinal stability augmentation systems (SAS) were designed by quadratic synthesis techniques to stabilize the unstable short period roots. By first ignoring and then including wing flexibility in the vehicle dynamic model, it was possible to investigate the effects of wing flexibility in the design of SAS's when significant dynamic coupling exists, and the effect of the method of control law implementation on system dynamics.

By adding an additional control surface, in this case a full-span trailing edge wing flaperon, other potential improvements in active aircraft control system design were also addressed. These improvements include the use of an active system to augment the flexible wing dynamics and an integrated design which simultaneously stabilizes the aircraft while reducing control activity of both the canard and flaperon.

This paper is organized as follows: The methodology used to model flexible aircraft longitudinal motion is discussed, together with the technique used to develop and implement the longitudinal stability augmentation control laws. A discussion of the results from a rigid-body control synthesis, then of the integrated approach, follows.

Methodology

The modeling technique for obtaining state variable representations of flexible aircraft[6] and the control synthesis method are summarized as follows. A mean reference axis coordinate system, with its origin located at the deformed aircraft instantaneous center of gravity, was defined. Structural deformations relative to this mean reference axis were expressed in terms of the free-free normal vibration modes. Generalized force expressions for the particular flight condition were calculated assuming quasisteady, incompressible aerodynamics. The inertial motion of the unrestrained aircraft center of gravity was expressed in terms of mean reference axis coordinates, and a set of nonlinear, differential equations describing the motion of the aircraft was obtained. These nonlinear equations were linearized using small perturbations about a steady-state flight condition.

The linearized equations defining the motions of the mean reference axis and wing elastic deformations may be written in matrix first-order form as

$$\begin{bmatrix} \dot{x}_R \\ \dot{x}_E \end{bmatrix} = \begin{bmatrix} A_R & A_{RE} \\ A_{ER} & A_E \end{bmatrix} \begin{bmatrix} x_R \\ x_E \end{bmatrix} + \begin{bmatrix} B_R \\ B_E \end{bmatrix} u \qquad (1)$$

where the subscript R denotes mean-reference-axis subsystem equations, and the subscript E denotes wing elastic (flexible) subsystem equations of motion. Although the selection of state variables is not unique, one could choose, for example, $x_R = (u_0, \alpha, \theta, \dot{\theta})^T$, and $x_E = (\eta_1, \dot{\eta}_1, \ldots, \eta_n, \dot{\eta}_n)^T$ where η_i is the generalized coordinate of the ith elastic mode and n is the number of elastic modes modeled, $u = (\delta_1, \ldots, \delta_m)$ where m is the number of control surfaces, and A and B are the $(2n+4 \times 2n+4)$ and $(2n+4 \times m)$ coefficient matrices, respectively.

Presented as Paper 82-1544 at the AIAA Guidance and Control Conference, San Diego, Calif., Aug. 9-11, 1982; submitted Aug. 26, 1982; revision received June 22, 1983.

*Graduate Student, School of Aeronautics and Astronautics. Member AIAA.

†Associate Professor, School of Aeronautics and Astronautics. Associate Fellow AIAA.

‡Professor, School of Aeronautics and Astronautics. Member AIAA.

Note in this formulation that if the structural degrees of freedom are not included, the equations reduce directly to

$$\dot{x}_R = A_R x_R + B_R u \tag{2}$$

or the state space equations of longitudinal motion for a rigid aircraft.

Table 1 lists the physical characteristics of a generic, forward-swept wing aircraft with a rigid fuselage and flexible wings.

The differential equations describing the longitudinal equations of motion, including the first wing bending mode, are developed in the form of Eq. (1), where the state vector x is now defined as $x=(u_0,\ \alpha,\ \theta,\ \dot{\theta},\ Z_T,\ \dot{Z}_T)^T$. Note that the elastic state Z_T is relative wing tip displacement (nondimensionalized by the wing semispan) associated with the first elastic mode, and u_0 is forward velocity perturbation, nondimensionalized by the steady-state vehicle flight velocity. The control vector u is $u=(\delta_a,\ \delta_c)^T$, where δ_a is the deflection of a full-span trailing edge wing flaperon, and δ_c is the deflection of the canard control surface.

Shown in Fig. 1 are the eigenvalue locations of the aircraft attitude and wing bending dynamics in the complex upper half-plane as a function of velocity (a velocity root locus). The flight velocities at sea level corresponding to labeled points in Fig. 1 are listed in Table 2 for reference. One real root associated with the aircraft pitch attitude is unstable for all velocities.

The unstable root of Fig. 1 can be stabilized using a variety of stability augmentation approaches. In this study, systems were designed to provide good "inner-loop" or attitude dynamics through quadratic synthesis of a pitch-rate-command augmentation system.[7]

To use this approach, cockpit stick deflection is taken as commanded pitch rate, and is modeled as a first-order Gauss-Markov random process by the relation

$$\dot{\delta}_s = \frac{1}{\tau_n}\delta_s + v \tag{3}$$

The constant τ_n can be related to the pilot's neuromuscular dynamics, and actually affects only the stick gains in the control law. The zero-mean Gaussian white noise v represents the unknown commanded stick input of the pilot. Adding this equation to the flexible aircraft equations by augmenting the state vector to include $\dot{\theta}_c$ $(=\delta_s)$, a quadratic performance index can be written as the expected value of the mean-square pitch-rate error and control activity,

$$J = E\left\{ \lim_{T\to\infty} \frac{1}{T}\int_0^T [(\dot{\theta}-\dot{\theta}_c)^2 + \rho(\gamma\delta_a^2 + \beta\delta_c^2)]\,dt \right\} \tag{4}$$

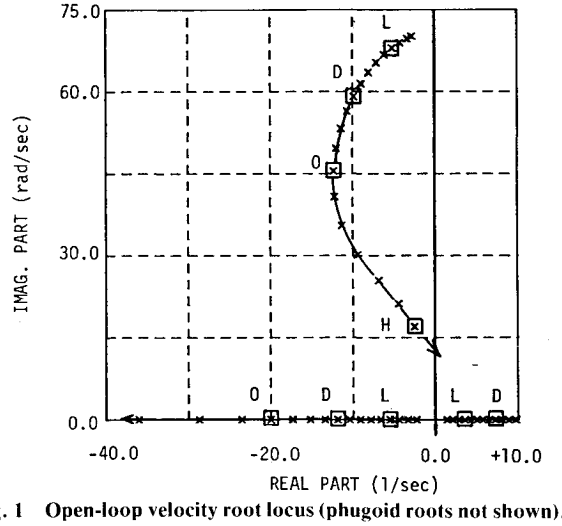

Fig. 1 Open-loop velocity root locus (phugoid roots not shown).

where $\dot{\theta}$ is actual aircraft pitch rate and $\dot{\theta}_c$ is commanded aircraft pitch rate, ρ is a parametric weighting factor, and γ and β are constants. The control law that minimizes J is the solution to the standard steady-state linear stochastic regulator,[8] a linear combination of the system states, $u=Gx$.

The optimal control law, expressed in terms of the state vector including the commanded pitch rate, is

$$u = [G_x G_{\dot{\theta}_c}] \begin{bmatrix} x \\ \dot{\theta}_c \end{bmatrix} = G_x x + G_{\dot{\theta}_c}\delta_s \tag{5}$$

The augmented aircraft equations of motion resulting from state feedback are, of course,

$$\dot{x} = (A + BG_x)x + BG_{\dot{\theta}_c}\delta_s \tag{6}$$

where G_x is the $(m\times 2n+4)$ state gain matrix.

In many cases, however, other measured outputs which are functions of the system states and controls are actually used as the feedback variables. These outputs may be expressed as

$$y = Cx + Du \tag{7}$$

where C and D are coefficient matrices which are functions of the flight condition. The gains G_y on the output feedback measurements, or $u=G_y y$, are found from the state gains G_x above using the relationship

$$u = (I + G_x C^{-1} D)^{-1} G_x C^{-1} y = G_y y \tag{8}$$

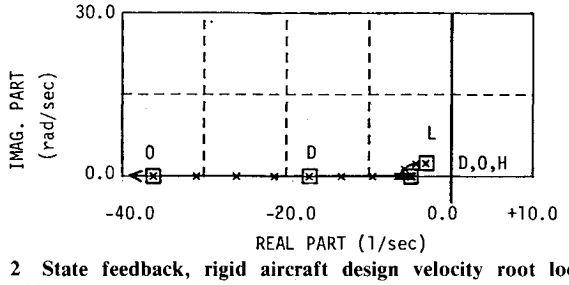

Fig. 2 State feedback, rigid aircraft design velocity root locus (phugoid roots not shown).

Table 1 Aircraft properties

Mass	496.9 slugs
Pitch inertia	42,646.0 slug ft^2
Wing semispan	13 ft
Wing sweep angle	30 ° forward
Wing surface area	180 ft^2
Wing taper ratio	1.0
Wing aspect ratio	3.75
Wing chord	6.93 ft
Canard surface area	34 ft^2
Canard hinge (fuselage station)	380
Wing root midchord (fuselage station)	550
Static margin	−34% mac
Wing bending frequency	69.5 rad/s
Wing torsion frequency	212.9 rad/s

Table 2 Figure labels and flight velocities

Label	Velocity, ft/s
L (low)	500
D (design)	1000
O (off-design)	1400
H (high)	2000

One real root associated with the aircraft pitch attitude is unstable for all velocities.

assuming C^{-1} exists. The augmented aircraft equations of motion are then given by

$$\dot{x} = [A + B(I - G_y D)^{-1} G_y C]x + BG_{\theta_c} \delta_s \qquad (9)$$

The two methods of implementation mathematically give the same augmented dynamics at the design flight condition, but not at other flight conditions.

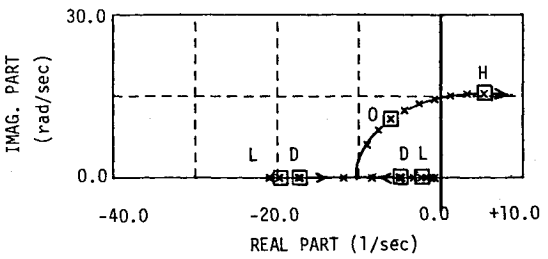

Fig. 3 Output feedback, rigid aircraft design velocity root locus (phugoid roots not shown).

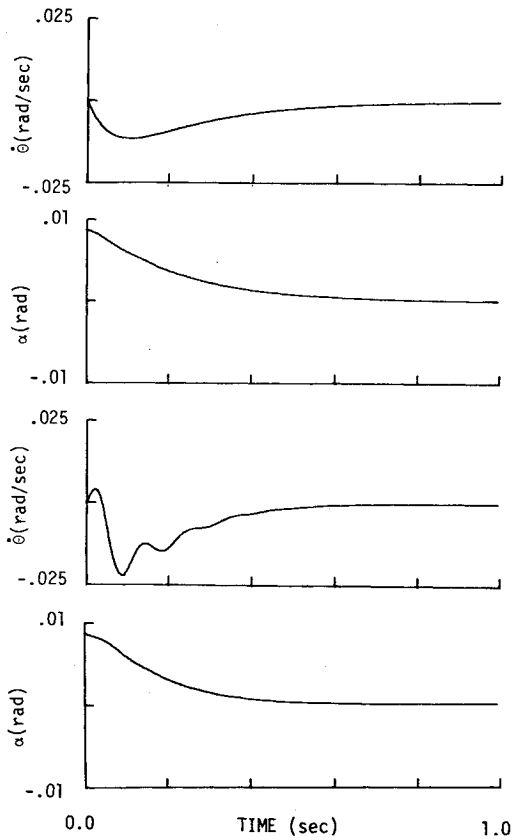

Fig. 4 Rigid and flexible aircraft pitch rate and angle-of-attack time responses (1000 ft/s).

Table 3 Rigid-body gains and eigenvalues

State	Gain
u_0	7.00×10^{-3}
α	-1.908
θ	-9.011×10^{-3}
$\dot{\theta}$,s	-3.144
$\dot{\theta}_c$,s	8.123×10^{-2}
Mode	**Eigenvalue**
Short period	$-17.23, -4.78$
Phugoid	$-0.008 \pm j0.044$

Rigid-Body Augmentation

Rigid-Body Synthesis

Frequently aircraft stability augmentation synthesis does not consider flexible aircraft dynamics, especially in the preliminary design stage. If there is wide frequency separation between the rigid-body and structural dynamic modes, and if the attitude dynamics then are dominated by the rigid-body modes, this is an acceptable approach for conventional aircraft. This section will show that such an approach on a FSW aircraft can lead to undesirable results.

Consider a canard as the only control surface to be used, and note that the equations of motion given by Eq. (1) reduce to those of Eq. (2) when the flexibility of the wing is ignored, where u is now simply δ_c. Expanding the state vector by the addition of the commanded pitch rate [Eq. (3)], the control laws which minimize the cost function J given by Eq. (4) with $\gamma = 0$, $\beta = 1$ for various levels of control system authority (varying control weight ρ) were obtained. Using the resulting gains and state feedback, the aircraft was augmented according to Eq. (6) over the same range of velocities as in Fig. 1. The velocity root locus is shown in Fig. 2 for one (fairly low) level of control authority (gains obtained for $\rho = 25$). The short period roots remain real and stable over the range of velocities. Table 3 lists the gains at the design flight condition, and the resulting augmented eigenvalues.

Now consider control law implementation using the measured outputs $y^T = (u_0, n_z, \theta, \dot{\theta})$, where

$$y = C_R x_R + Du \qquad (10)$$

and n_z is cockpit normal acceleration in g's. The output gains were computed from Eq.(8) using the state feedback gains of Table 3, noting again that the coefficient matrices C and D are dependent on flight condition, with implications previously cited. The output-feedback implementation [Eq. (9)] velocity root locus is shown in Fig. 3. At off-design dynamic pressures, the effect of the different implementation is evident

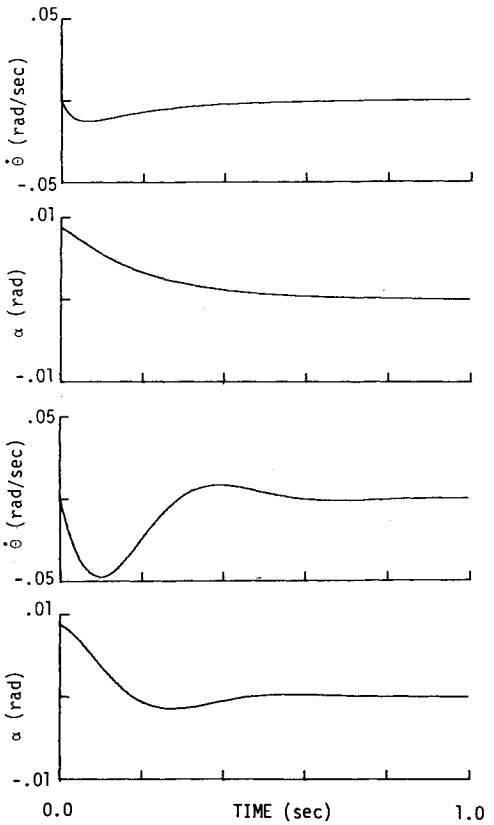

Fig. 5 Rigid and flexible aircraft pitch rate and angle-of-attack time responses (1400 ft/s).

in the difference between the eigenvalue locations of the output feedback (Fig. 3), and the state feedback implementations (Fig. 2).

Smooth, well damped behavior is exhibited in the pitch-rate and angle-of-attack time responses to an impulsive 8.73 ft/s gust, as shown in the top half of Fig. 4. These two histories correspond to the design flight condition ($\rho = 25$, 1000 ft/s), while the top two traces in Fig. 5 are the time responses at an off-design flight condition ($\rho = 25$, 1400 ft/s) with the same gains (note the change of scale between the two sets of figures for the purpose of later comparisons).

The Effects of Flexibility

The results just presented assumed a rigid aircraft configuration. Considered now is implementation of the above control laws on the aircraft including flexibility. Looking at output feedback implementation, the output equations are modified to include the elastic states

$$y = [C_R C_E] \begin{bmatrix} x_R \\ x_E \end{bmatrix} + [D]u \tag{11}$$

where C is now $(4 \times 2n + 4)$ matrix of coefficients which includes the wing aeroelastic effects. The vector y is defined as before, i.e., $y^T = (u_0, n_z, \theta, \dot{\theta})$, and the previously calculated gains, G_y, are used. The control law, when implemented, includes the effects of the elastic states, as well as the rigid-body states

$$u = (I - G_y D)^{-1} G_y C \begin{bmatrix} x_R \\ x_E \end{bmatrix} \tag{12}$$

where $C = [C_R C_E]$.

Locations of augmented aircraft attitude and wing bending mode eigenvalues are shown in Fig. 6 for the same range of velocities previously considered. Figure 6, with gains obtained when $\rho = 25$, shows that not only are the "short period" roots different for off-design conditions when compared with Fig. 3, but that the roots at the design condition have also been modified.

Note that in the case shown, the "rigid-body" branch in the root locus (Fig. 6) goes unstable at the higher velocities, but at a lower value than the case shown in Fig. 3. For other center of gravity locations and/or other control implementations, the "wing bending" branch goes unstable instead, similar to the behavior reported by Miller et al.[3] and Weisshaar et al.[4,5]

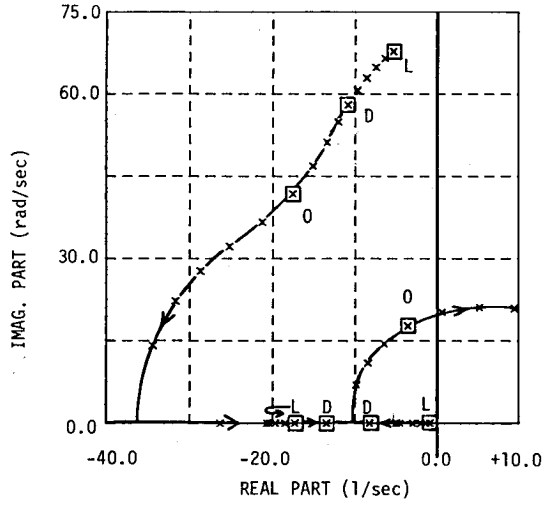

Fig. 6 Output feedback, flexible aircraft implementation velocity root locus (phugoid roots not shown).

The significance of the elastic mode in the aircraft time responses to the same sharp vertical gust of 8.73 ft/s is shown in Figs. 4 and 5. The upper curves in Fig. 4 are the responses discussed previously, based on a rigid aircraft analysis. The lower curves show the actual $\dot{\theta}$ and α responses when the same control gains are implemented via output feedback on the flexible aircraft. The differences in the time responses of Fig. 4 can be explained in terms of the eigenvalues and eigenvectors of Table 4. Comparing the rigid and flexible body analyses, the flexible aircraft eigenvectors have large structural displacement and rate contributions in all modes. As a result, the so-called "short period" mode is no longer purely an attitude mode for the flexible vehicle. Furthermore, although this lower frequency mode still dominates attitude response, the other mode contributes significantly to pitch rate.

The situation is even more pronounced when considering the time responses at the higher velocity off-design flight condition (1400 ft/s). The character of the time responses is completely changed from that of the rigid vehicle, as shown in the lower curves of Fig. 5. Note too the magnitude of the elastic vehicle response in the light of the scale change between Figs. 4 and 5.

Analysis

The flexible aircraft dynamics can be further investigated by considering the observability (with respect to important physical responses) and controllability[9] of the unaugmented attitude and wing bending dynamics.

Defining the transformation $x = Tq$, where the matrix T is the complex modal matrix formed from the eigenvectors of the state-space model of the open-loop (unaugmented) flexible aircraft, the equations of motion of the aircraft can be expressed in vehicle modal coordinates as

$$\dot{q} = T^{-1} A T q + T^{-1} B u \tag{13}$$

where $T^{-1}AT$ is a diagonal matrix consisting of the eigenvalues of A. With each eigenvector in T normalized to unity length, the elements of $T^{-1}B$ reveal the relative controllability of a dynamic mode with respect to the control surfaces.

Relative observability of the dynamic modes in the controlled variable $(\dot{\theta} - \dot{\theta}_c)$ in the cost function J of Eq. (4) is an indication of the influence the minimizing control law will have on those modes. Likewise, observability of the modes in wing bending deformation, Z_T, is equally important. The observability measure, in this analysis, is determined directly from the eigenvector information. The controlled variable $p = (\dot{\theta} - \dot{\theta}_c)$ may be expressed in terms of the states of the aircraft as

$$p = Ex \tag{14}$$

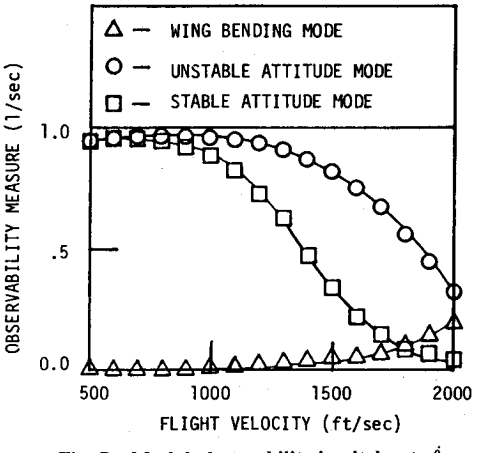

Fig. 7 Modal observability in pitch rate $\dot{\theta}$.

Table 4 Eigenvalue and eigenvector data

	Rigid design, rigid implementation		
State/root	−17.23	−4.78	
u_0	7.64×10^{-4}	0.002	
α	−0.076	−0.369	
θ	−0.058	−0.190	
$\dot{\theta}$	0.995	0.910	
	Rigid design, flexible implementation		
State/root	−13.56	−8.24	-10.87 ± 57.94
u_0	8.49×10^{-4}	0.001	2.00×10^{-5} arg 9.6 deg
α	−0.093	−0.169	0.002 arg 167.8 deg
θ	−0.066	−0.103	0.001 arg 168.4 deg
$\dot{\theta}$	0.892	0.850	0.080 arg 67.8 deg
Z_T	0.032	0.059	0.017 arg 34.8 deg
$\dot{Z}_T$	−0.436	−0.484	0.996 arg 135.5 deg

Table 5 Flexible aircraft design eigenvalues and gains

	Canard only	Flaperon only	Canard/flaperon
	$-9.88\pm j\,59.1$	$-9.89\pm j\,59.1$	$-9.89\pm j\,59.1$
Eigenvalues	−17.84	−12.44	−18.13
	−5.26	−7.24	−5.32
State	Gains		
u_0	1.77×10^{-2}	-3.84×10^{-1}	$1.52\times10^{-2}/-6.17\times10^{-3}$
α	−1.98	5.21	−1.70/0.692
θ	-9.56×10^{-3}	9.52×10^{-3}	$-9.34\times10^{-3}/1.72\times10^{-3}$
$\dot{\theta}$	−0.32	0.67	−0.28/0.11
Z_T	1.95×10^{-4}	-3.63×10^{-4}	$1.77\times10^{-4}/-6.23\times10^{-5}$
$\dot{Z}_T$	-1.17×10^{-6}	-2.54×10^{-6}	$1.07\times10^{-6}/-3.35\times10^{-7}$
θ_c	8.17×10^{-2}	-3.81×10^{-2}	$8.50\times10^{-2}/-2.16\times10^{-2}$

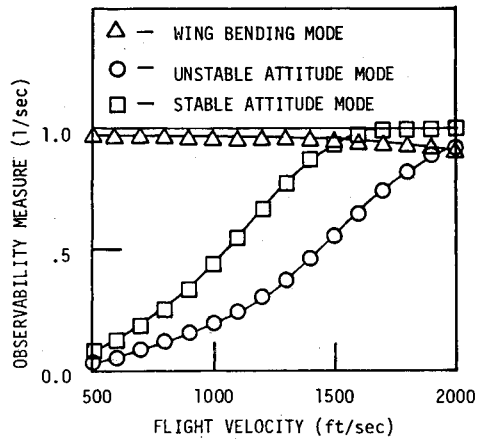

Fig. 8 Modal observability in wing tip bending rate $\dot{Z}_T$.

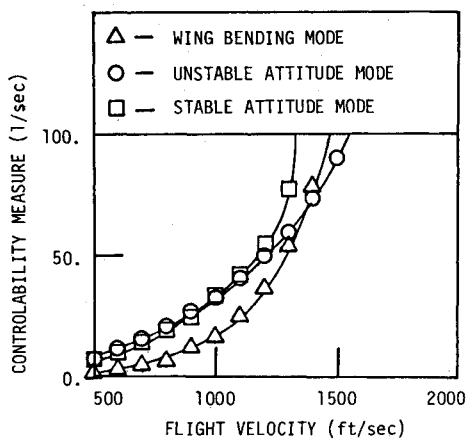

Fig. 9 Modal controllability of the canard.

where $E=(0,0,0,1,0,0,-1)$. From the modal transformation $x=Tq$, the variable p in terms of modal coordinates is

$$p=ETq \tag{15}$$

The elements of ET reflect directly relative observabilities of the dynamic modes in p.

Shown in Figs. 7 and 8 are the relative observabilities of the modes (associated with the complex, real stable, and real unstable eigenvalues) in $\dot{\theta}$ and $\dot{Z}_T$, respectively, for the unaugmented aircraft. The complex mode is nearly all wing bending, as it is almost unobservable in pitch rate and the observability measure for the mode in $\dot{Z}_T$ is near 1.0. However, an even more interesting result is the amount the real eigenvalue modes contribute to, or are observable in, wing bending displacement Z_T. As shown, above 1100 to 1200 ft/s the real modes contribute significantly to bending deformation, and they are no longer "pure attitude" or "short period" roots. Put another way, the "short period" mode now exhibits significant wing bending, along with vehicle attitude motion.

Furthermore, these modes (complex and real) are all highly controllable, and therefore highly modified through active control. This is shown in the plots of controllability measures for the four eigenvalues (modes) in Figs. 9 and 10, for the canard and flaperon respectively. Figure 9 shows that even if the canard is used as the only active control surface, the control authority this surface has over all the modes, including the complex wing-bending mode identified above, will cause the modes to be modified by control action. Therefore, designing control laws improperly or ignoring the bending mode can drastically alter all dynamic modes when they are implemented. This result leads to the time response variations in Figs. 4 and 5.

Integrated Designs

The previous results indicate that ignoring wing flexibility effects in the design of stability augmentation systems on

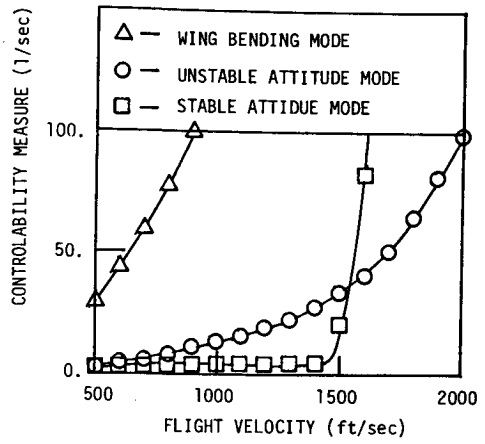

Fig. 10 Modal controllability of the flaperon.

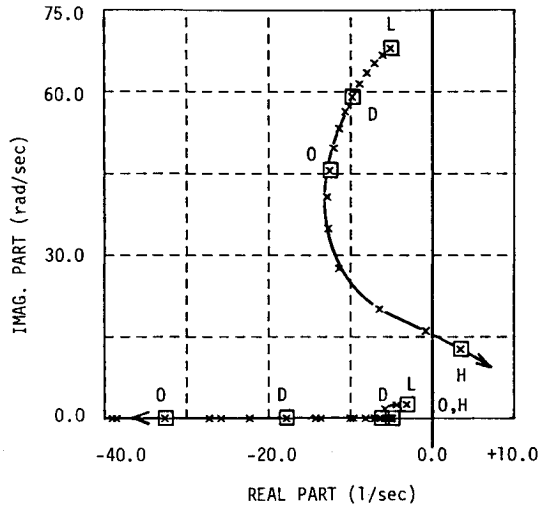

Fig. 11 Flexible aircraft design velocity root locus (phugoid roots not shown).

Table 6 RMS control surface activity

Canard only, rad	0.0180
Flaperon only, rad	0.0092
Canard and flaperon, rad	0.0173/0.0077

FSW aircraft can result in unexpected and undesirable aircraft dynamics. Using the flexible aircraft model of Eq. (1) with canard only, and again synthesizing the rate command augmentation system by minimizing the same cost functional J given by Eq. (4) as before, leads to the velocity root locus shown in Fig. 11 for gains obtained when $\rho = 25$. Comparing Fig. 11 with Fig. 6 shows a much more robust control system in the light of an increase in dynamic pressure before instability is reached as well as a shift in the mode of instability. Also it should be noted that the "short period" root locus branch of Fig. 11 is very similar to that of Fig. 2, the original rigid-body design, with the real roots in almost identical locations to those for the design condition (1000 ft/s).

Augmented aircraft time responses ($\rho = 25$) to the 8.73 ft/s impulsive gust are shown in Figs. 12 and 13 for the design case (1000 ft/s), and the off-design condition (1400 ft/s). Comparing these results with Figs. 4 and 5 shows the time responses are much closer to the original time response obtained in the rigid-body analysis, with the elastic mode contribution barely visible at the design condition. These results underscore the effectiveness of the canard alone in controlling not only the attitude but the wing bending mode as well.

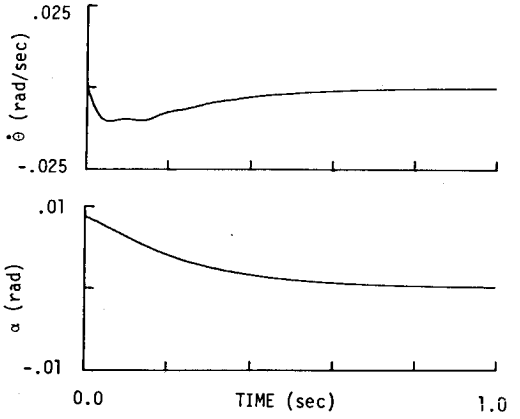

Fig. 12 Flexible aircraft pitch rate and angle-of-attack time responses (1000 ft/s).

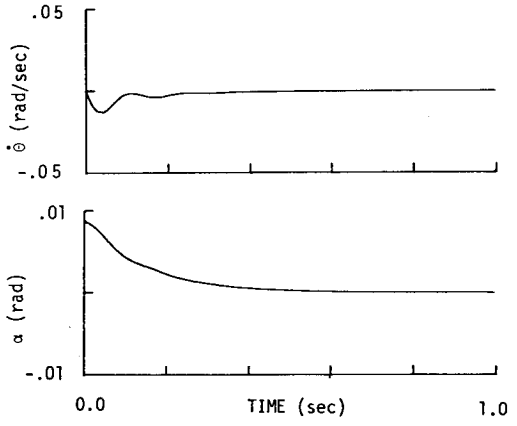

Fig. 13 Flexible aircraft pitch rate and angle-of-attack time responses (1400 ft/s).

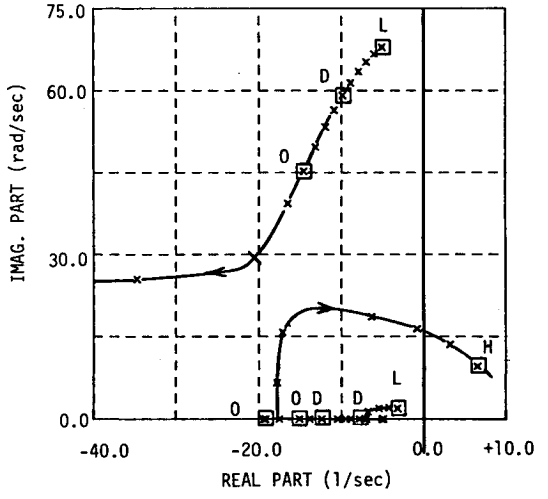

Fig. 14 Flexible aircraft design velocity root locus—flaperon control only (phugoid roots not shown).

Two final cases were considered that include the full span trailing edge flaperon as an active control surface. The inclusion of the flaperon was considered to determine if additional improvements could be obtained over those with the canard only. The first control system uses the flaperon as the only control surface, and the second uses both the canard and flaperon. Both cases are for gains obtained with $\rho = 25$. The gains for the flaperon and the canard/flaperon cases, as well as the canard only case, are given in Table 5.

The velocity root loci are shown in Figs. 14 and 15. Although flaperon control alone is capable of stabilizing the

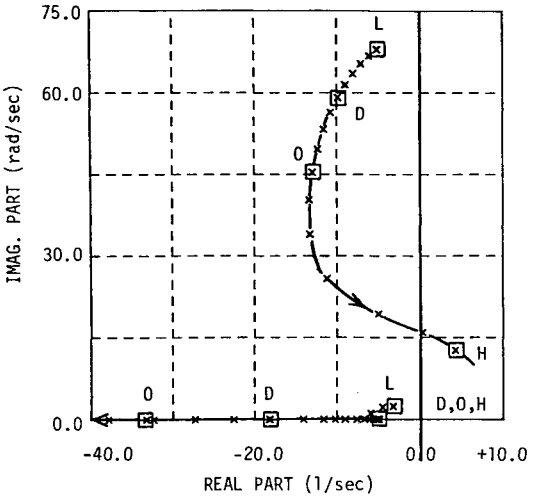

Fig. 15 Flexible aircraft design velocity root locus—canard and flaperon control (phugoid roots not shown).

system, Fig. 14 and the time response (not shown) indicate less desirable characteristics than the case with canard only. Comparing the time response for flaperon/canard control to those in Figs. 12 and 13 (canard only case) showed no further improvement. However, the relative "costs" of augmentation are reflected in the rms control surface activity for the system excited by a random control-stick input. These rms activities are listed in Table 6 for an excitation noise covariance $V = 0.061\ (\text{rad/s})^2$.

Indications are that for the rate-command SAS systems considered in this paper, little improvement is obtained by the addition of the active flaperon. Further modification of the wing bending dynamics through alteration of the cost function J is feasible, however, and would be most effectively accomplished via the flaperon. This topic is currently under investigation.

Conclusion

In this paper, some of the problems associated with the use of longitudinal stability augmentation on aircraft with strong interactions between the flight mechanic and structural dynamic degrees of freedom have been shown. Neglecting to include the wing flexibility in the dynamic model in design and evaluation results in significant differences between anticipated and actual eigenvalue locations and system response. By examining the controllability and observability of the various system modes it is possible to explain those differences, and such an analysis would appear to be appropriate before augmentation synthesis. Finally, it is noted that all the systems synthesized here were attitude rate-command systems, intended primarily for attitude augmentation. Through the addition of the rate of relative wing tip displacement in the cost function, an improved integrated attitude and structural mode control system could be developed.

Acknowledgments

This study was supported by the NASA Langley Research Center under NASA Grant NAG-1-157. Mr. J. R. Newsom is technical monitor.

References

[1]Krone, N. J. Jr., "Divergence Elimination with Advanced Composites," AIAA Paper 75-1009, Aug. 1975.

[2]Krone, N. J., Jr. "Forward Swept Wing Flight Demonstrator," AIAA Paper 80-1882, Aug. 1980.

[3]Miller, G. D., Wykes, J. H., and Brosnan, M. J., "Rigid Body-Structural Mode Coupling of a Forward Swept Wing Aircraft," AIAA Paper 82-0683, May 1982.

[4]Weisshaar, T. A., Zeiler, T. A., Hertz, T. J., and Shirk, M. H., "Flutter of Forward Swept Wings, Analyses and Tests," AIAA Paper 82-0646, May 1982.

[5]Weisshaar, T. A. and Zeiler, T. A., "Dynamic Stability of Forward Swept Wing Aircraft," AIAA Paper 82-1325, Aug, 1982.

[6]Gilbert, M. G., "Dynamic Modeling and Active Control of Aeroelastic Aircraft," Master of Science Thesis, School of Aeronautics and Astronautics, Purdue University, West Lafayette, Ind., Dec. 1982.

[7]Schmidt, D. K., "Quadratic Synthesis of Command Augmentation Flight Control Laws," submitted for publication to *Journal of Guidance, Control, and Dynamics.*

[8]Kwakernaak, H. and Sivan, R., *Linear Optimal Control Systems*, John Wiley and Sons, Inc., New York, N. Y., 1972.

[9]Brogan, W. L., *Modern Control Theory*, Quantum Publishers, Inc., New York, N. Y., 1974.